

www.acsami.org Forum Article

Dynamic Ablative Networks: Shapeable Heat-Shielding Materials

Kevin A. Stewart, Daniel P. DeLellis, Jacob J. Lessard, John F. Rynk, and Brent S. Sumerlin*



Cite This: https://doi.org/10.1021/acsami.2c22924



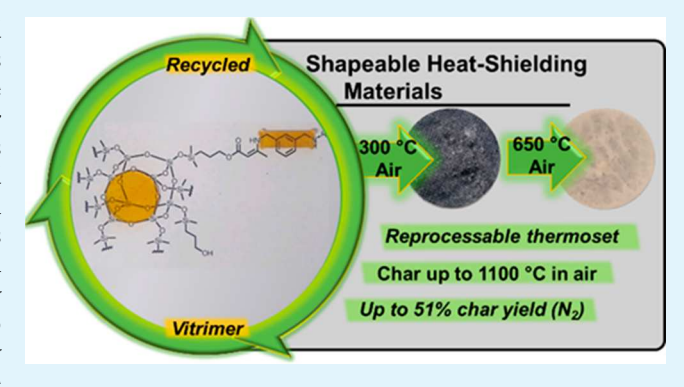
ACCESS

Metrics & More

Article Recommendations

s Supporting Information

ABSTRACT: Thermoset materials sacrifice recyclability and reshapeability for increased chemical and mechanical robustness because of an immobilized, cross-linked polymeric matrix. The robust material properties of thermosets make them well-suited for applications such as heat-shielding materials (HSMs) or ablatives where excellent thermal stability, good mechanical strength, and high charring ability are paramount. Many of these material properties are characteristic of covalent adaptable networks (CANs), where the static connectivity of thermosets has been replaced with dynamic cross-links. This dynamic connectivity allows network mobility while retaining cross-link connectivity to permit damage repair and reshaping that are traditionally inaccessible for thermoset materials. Herein, we report the



synthesis of hybrid inorganic—organic enaminone vitrimers that contain an exceptionally high weight percent of polyhedral oligomeric silsesquioxane (POSS)-derivatives. Polycondensation of β -ketoester-containing POSS with various diamine cross-linkers led to materials with facile tunability, shapeability, predictable glass transition temperatures, good thermal stability, and high residual char mass following thermal degradation. Furthermore, the char materials show notable retention of their preordained shape following decomposition, suggesting their future utility in the design of HSMs with complex detailing.

KEYWORDS: covalent adaptable networks, vitrimers, creep-resistance, ablatives, nanocomposites, POSS

■ INTRODUCTION

Owing to their permanently cross-linked structure, thermosets boast impressive resistance to chemical exposure and possess dimensional, mechanical, and thermooxidative stability. These features make thermosets exceptional candidates for highperformance materials in aerospace applications such as heatshielding materials (HSMs).^{2,3} HSMs are responsible for impeding the transmission of thermal energy to an underlying protected surface, such as the inner surface of a solid rocket motor casing or components near engines or heat zones (Figure 1). HSMs must also be capable of withstanding normal operating and storage conditions, often for extended periods of time, prior to a thermal event. A variety of materials serve as the basis for such thermal protection systems and their binders, including metals, inorganic polymers or ceramics, and organic polymer intumescents or ablatives. 4-8 Polymeric ablative insulators impart thermal protection to an underlying layer by virtue of a discrete pyrolysis event that produces a residual and inert char layer that protects from further thermooxidative stress.^{9,10} Some of the most utilized polymeric ablative insulators include phenolic resins, nitrile butadiene rubber (NBR), ethylene-propylene diene rubber (EPDM), and silicone elastomers. 11-13 These materials are typically loaded with a stabilizing filler (SiO2, aramid or carbon fibers, and various ceramic precursors) to augment the material integrity

before/during operational use and to boost the charring ability. $^{14-16}$

Although polymeric ablatives are typically thermoset materials, the intrinsic permanent structure of traditional cross-linked materials complicates both material recycling and the ability to access complex shapes after synthesis. Recent research in covalent adaptable networks (CANs) potentially allows such drawbacks to be mitigated. 17 CANs are polymer networks comprised of covalent cross-links that are dynamic/ reversible when exposed to a specific stimulus, the most common being heat. Upon introduction of heat and/or mechanical force (e.g., compression or shear), cross-link exchange dissipates thermal or mechanical energy through macroscopic flow. These networks possess the robustness of thermosets while featuring the shapeability and recyclability of thermoplastics. 18,19 CANs are typically segregated into two distinct classes depending on their mechanism of cross-link exchange.²⁰ Dissociative CANs are governed by exchange in which cross-links are in equilibrium with their individual

Special Issue: Applied Supramolecular Materials

Received: December 27, 2022 Accepted: February 24, 2023



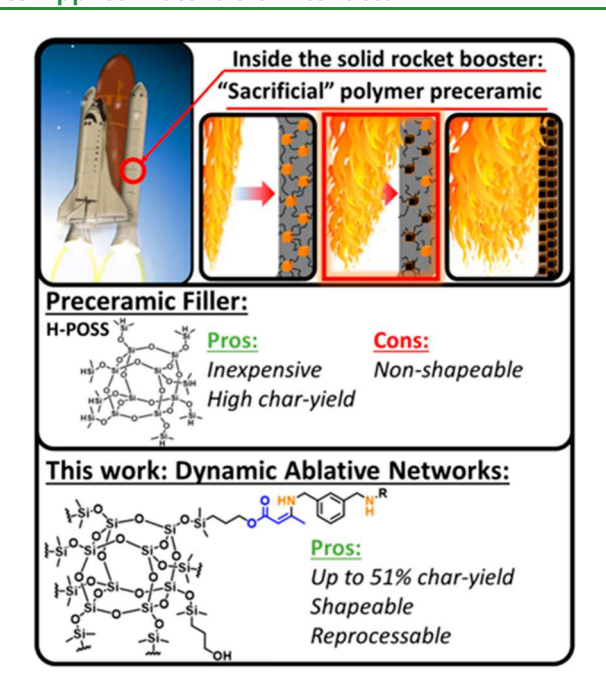


Figure 1. (Top) Simplified diagram of the inside of solid rocket booster (SRB): fuel consumption causing the heat front to propagate toward the ablative HSM layer (orange cubes), causing pyrolysis (orange and black cubes) and eventual charring, leading to an inert, protective barrier (black cubes) (left to right). (Middle) Commercially available "OctaSilane-POSS" (H-POSS), a convenient POSS-like scaffold with high charring ability. (Bottom) Current work using H-POSS to synthesize vitrimer networks of shapeable, high-charring capabilities.

reactive partners and the covalent adduct formed between them. Dissociative CANs typically, ^{21–24} though not always, ^{25,26} demonstrate rapid decreases in viscosity at elevated temperatures. Associative CANs, often referred to as "vitrimers," operate by a degenerate exchange reaction in which reactive moieties within the network react with existing cross-links to form a new cross-link and liberate an identical reactive group. ^{27–29} This process leads to predictable changes in viscosity and allows for the cross-link density to be well maintained during (re)processing.

Vitrimers can operate by a wide variety of dynamic chemistries to afford associative cross-link exchange. However, many vitrimer chemistries require external catalysis to facilitate appreciably rapid exchange, potentially increasing the overall cost and decreasing the lifetime of the networks through catalyst degradation or leaching.^{30–33} On the other hand, catalyst-free systems such as silyl ether exchange, dioxaborolane and imine metathesis, and transamination of enaminones accomplish facile bond exchange without the necessity of additives. 34-39 Enaminone transamination has led to a burgeoning collection of vitrimer materials due to commercial availability or facile synthesis of β -ketoester-containing monomers and multiamine building blocks. 40-42 Recently, our group has capitalized on this exchange mechanism in combination with the straightforward synthesis of linear polymers containing 2-(acetoacetoxy)ethyl methacrylate (AAEMA), a reactive β -ketoester-containing monomer. 43,44 Leveraging controlled radical polymerization, we have demonstrated that modifying the architecture and composition of cross-linkable macromolecular building blocks allows the rheological behavior of the final vitrimers to be tuned. 45,46

Despite the many advantages of CANs, the dynamic nature of their cross-links can often result in mechanical properties that are inferior to static thermosets. Combining the dynamicity of vitrimers with the reinforcement of discrete fillers in composite materials has become an increasingly attractive platform for mitigating such drawbacks. 47 Including fillers in typical commercial thermosets allows facile augmentation of material properties such as tensile strength, thermal stability, and thermal or electrical conductivity.4 Fillers including derivatized cellulose and chitosan, carbon fiber and carbon nanotubes, graphene, and silica nanoparticles have also been implemented into a variety of vitrimer materials. 49-55 Although these nanoparticle fillers improve certain material properties, factors such as filler content, efficient dispersion, and phase separation can be difficult to optimize. In many cases, there are diminishing returns on material enhancement, as high degrees of filler loading or filler incompatibility in the matrix can hinder efficient topological rearrangements of the vitrimer network.5

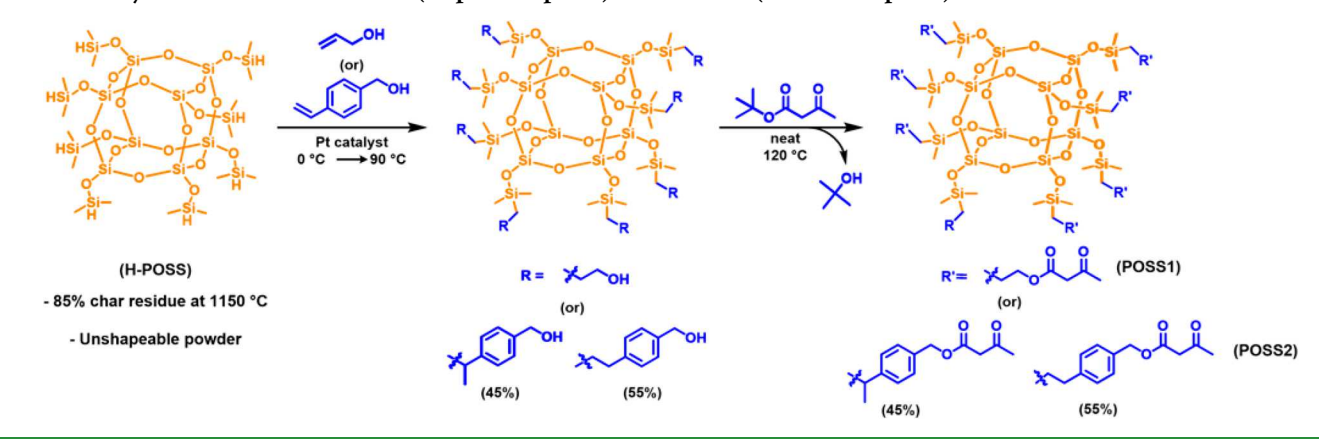
Polyhedral oligomeric silsesquioxanes (POSS) are nanoscale inorganic cage-like molecules that serve as convenient frameworks for the production of high-performance nano--60 Facile derivatizacomposites and preceramic polymers.⁵⁷ tion with organic substituents at the Si-vertices of POSS cages enables efficient dispersion in a range of polymeric matrices, with the rigid nanosilica core imparting thermochemical stability. Such features make POSS an appealing framework for fabricating vitrimers with high incorporation of inorganic fillers, thereby yielding materials that combine dynamicity with stability. However, POSS-based vitrimers have only recently garnered attention as promising platforms for composite CANs. 61-66 Herein, we report the incorporation of novel β ketoester-functionalized POSS cages to form nanocomposite vitrimers which, to the best of our knowledge, possess the highest weight percent POSS to date in vitrimer materials. The high degree of POSS cross-linked with various diamines led to vitrimers with tunable viscoelastic flow and glass transition temperatures (Tg), excellent creep resistance, and highperformance charring capabilities, potentially making these materials promising as HSMs with tailorable shapes.

EXPERIMENTAL SECTION

Materials. OctaSilane POSS (H-POSS, Hybrid Plastics, 98%), allyl alcohol (Acros Organics, 99+%), platinum(0)-1,3-divinyl-1,1,3,3-tetramethyldisiloxane complex solution in xylene (Karstedt's catalysts, Millipore Sigma, 2% Pt), 4-vinylbenzyl chloride (VBC, Millipore Sigma, 90%), sodium acetate (ACS grade, Millipore Sigma), tert-butyl acetoacetate (TBAA, Millipore Sigma, 98%), anhydrous toluene (ACS grade, Fisher), dimethyl sulfoxide (DMSO, ACS grade, Fisher), tetrahydrofuran (THF, ACS grade, Fisher), 200 proof ethanol (ACS grade, Fisher), xylylene diamine (XDA, Millipore Sigma, 99%), hexamethylenediamine (HMDA, Millipore Sigma, 98%), and 1,12-diaminododecane (DADD, Millipore Sigma, 98%) were used as received.

Synthesis of Octapropanol POSS (OP-POSS). OctaSilane POSS (H-POSS, 5.09 g, 1.00 equiv) was added to a 25 mL round-bottomed flask (RBF) containing 17 mL of anhydrous toluene. A stir bar was added, and the RBF was charged with 3.06 mL of allyl alcohol. The reaction vessel was placed in an ice bath and allowed to stir for 10 min. Slowly, 45.0 μ L of Karstedt's catalyst was added dropwise to the reaction vessel and, upon complete addition, the solution was allowed to stir for 15 min. The reaction vessel was removed from the ice bath, equipped with a reflux condenser, and stirred in a 90 °C oil bath for 22 h. The biphasic solution was removed from heat, allowed to cool to room temperature, and diluted

Scheme 1. Synthetic Route to POSS1 (Aliphatic Spacer) and POSS2 (Aromatic Spacer) Monomers from H-POSS



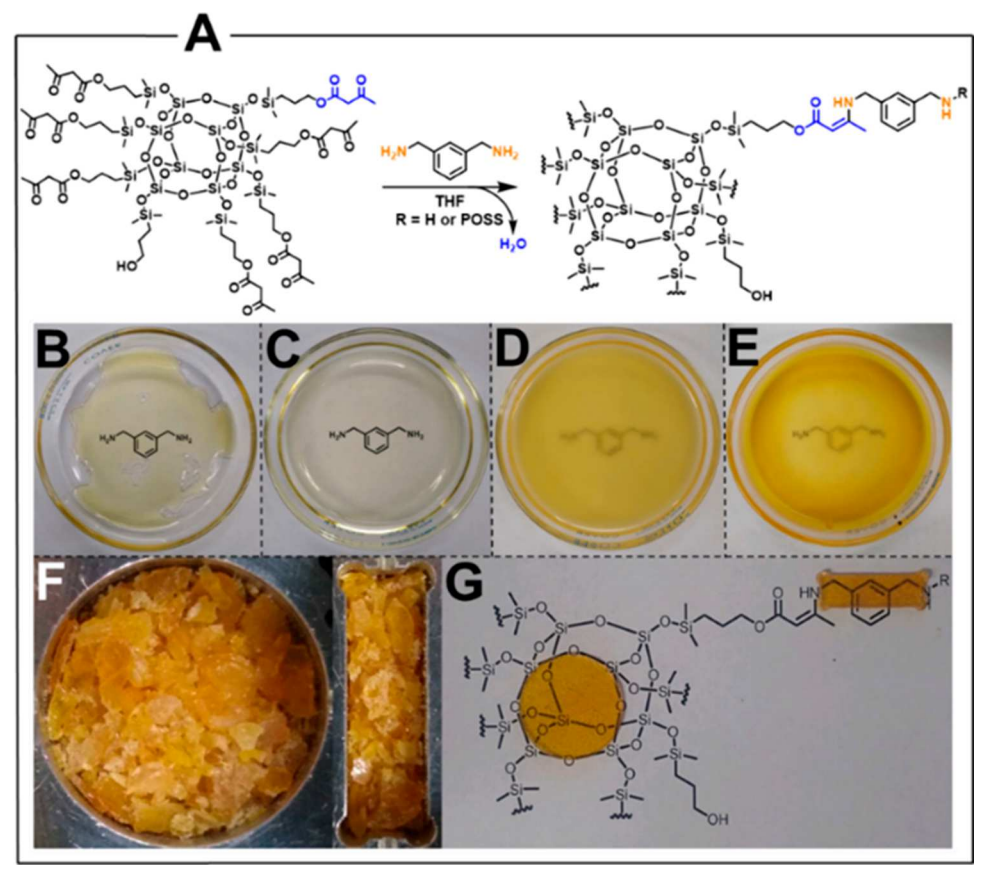


Figure 2. X1 vitrimer formation and processing. (A) Scheme of network formation via condensation of POSS1 (β -ketoester functionalized cage with an aliphatic spacer) with diffunctional amine m-xylyenediamine (XDA). POSS1 oil product (B) before and (C) after solubilizing in THF. (D) Organogel formation 15 min after addition of XDA cross-linker. (E) Vitrimer film after curing under vacuum at 85 °C for 6 h. (F) Pulverized vitrimer shards before processing and (G) the reformed vitrimer after processing at 160 °C under vacuum.

with 20 mL of acetone. A dark gray precipitate was gravity filtered and the filtrate was rotary evaporated to dryness to give a clear, viscous yellow oil (7.23 g, 97.5%). ¹H NMR (CDCl₃, 600 MHz): δ 3.62–3.55 (t, 16H), 1.70–1.60 (p, 16H), 0.65–0.58 (t, 16H), 0.22–0.18 (s, 48H); ¹³C NMR (CDCl₃, 600 MHz): δ 65, 26, 13, –0.9 (Figure S1A-R)

Synthesis of 4-Vinylbenzyl Alcohol (VBA). 4-Vinylbenzyl chloride (10.3 mL, 1.00 equiv) was added to a 50 mL RBF containing 40 mL of DMSO. A stir bar was added, and 6.58 g of sodium acetate was added. The reaction vessel was capped and placed in a 40 $^{\circ}$ C oil bath for 24 h. The reaction was then cooled to room temperature and poured into 60 mL of DI water. The aqueous solution was extracted with ethyl acetate (3 \times 20 mL), combined, dried with sodium sulfate,

and rotary evaporated to a clear, colorless liquid. The product was then reconstituted in 30 mL of ethanol, to which 25 mL of 20% NaOH was added. The reaction vessel was equipped with a condenser and placed in a 70 °C oil bath for 4 h. The solution was allowed to cool to room temperature and extracted with ethyl acetate (3 \times 50 mL), washed with DI water (2 \times 100 mL) and brine (3 \times 75 mL). The organic layers were combined, dried with sodium sulfate, and rotary evaporated to give a brownish red oil. The product was purified via column chromatography (2:1 hexanes/ethyl acetate) as a mobile phase to give a clear, slightly colored oil (4.920 g, 50.4%). $^1{\rm H}$ NMR (CDCl $_3$, 600 MHz): δ 7.50–7.10 (m, 4H), 6.85–6.45 (m, 1H), 5.80–5.50 (d, 1H), 5.25–5.10 (d, 1H), 4.50 (s, 2H), 3.10–3.00 (s, 1H) (Figure S4).

ACS Applied Materials & Interfaces

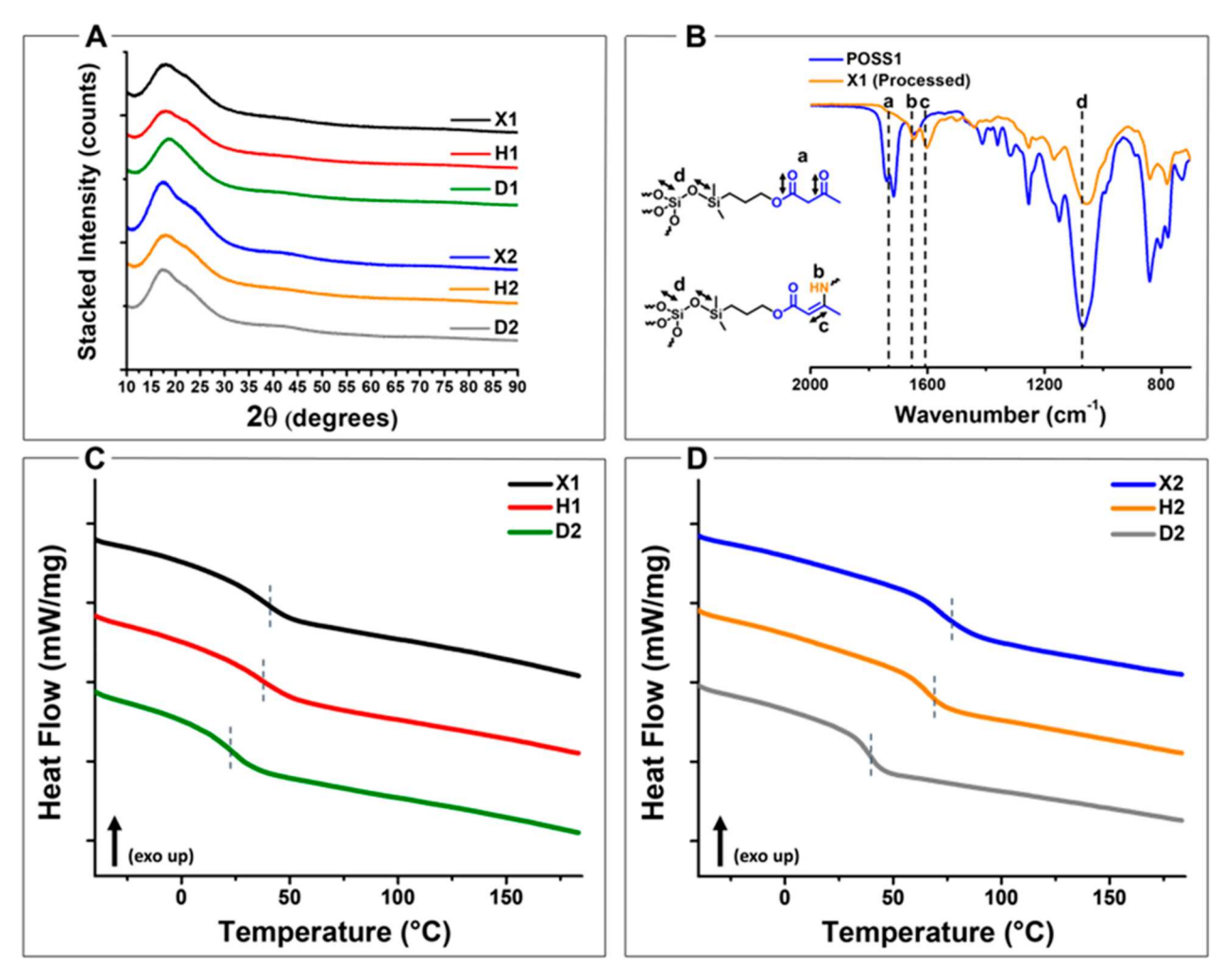


Figure 3. Nanocomposite vitrimer characterization. (A) X-ray diffraction (XRD) patterns of POSS vitrimers showing amorphous character. (B) Overlayed FTIR spectra of POSS1 (β-ketoester functionalized cage with aliphatic spacer) vitrimer cross-linked with m-xylyenediamine (X1) showing the characteristic stretches of the enaminone functional group and consumption of β-ketoester carbonyl. (C) Stacked differential scanning calorimetry (DSC) plots with marked T_g values of POSS1 and (D) POSS2 (β-ketoester functionalized cage with an aromatic spacer) vitrimers.

Synthesis of Octabenzylalcohol POSS (OBA-POSS). 4-Vinylbenzyl alcohol (4.92 g, 36.6 mmol, 9.00 equiv) was added to a 50 mL RBF containing 17 mL of anhydrous toluene. H-POSS (4.12 g, 4.05 mmol, 1.00 equiv) was added and the solution was stirred in an ice bath for 10 min. Slowly, 45.0 µL of Karstedt's catalyst was added dropwise to the reaction vessel and, upon complete addition, the solution was allowed to stir for 15 min. The reaction vessel was removed from the ice bath, equipped with a reflux condenser, and stirred in a 90 $^{\circ}\text{C}$ oil bath for 20 h. The biphasic solution was removed from heat, allowed to cool to room temperature, and diluted with 20 mL of acetone. A dark gray precipitate was gravity filtered and the filtrate was rotary evaporated at elevated temperatures for 2 h to give a dark, extremely viscous brown oil with a slight excess of VBA. The product was used without further purification (8.23 g, 97.2%). ¹H NMR (CDCl₃, 600 MHz): δ 3.62–3.55 (t, 16H), 1.70–1.60 (p, 16H), 0.65-0.58 (t, 16H), 0.22-0.18 (s, 48H) (Figure S5).

Synthesis of POSS1. *Tert*-butyl acetoacetate (TBAA, 7.12 mL, 42.9 mmol, 8.80 equiv) was added to a 50 mL RBF containing OP-POSS (7.23 g, 4.88 mmol, 1.00 equiv) and a stir bar. The RBF was equipped with a distillation apparatus and stirred at room temperature for 10 min. After, the RBF was submerged in a 120 °C oil bath and stirred for 18 h. The reaction mixture was then placed under reduced pressure to vacuum distill off the excess TBAA at 125 °C for 2 h, yielding a clear, very viscous yellow oil (10.2 g, 96.8%). ¹H NMR (CDCl₃, 600 MHz): δ 4.18–4.10 (t, 14 H), 3.45–3.40 (s, 14H),

2.28-2.25 (s, 21 H), 1.70-1.60 (p, 16H), 0.65-0.58 (t, 16H), 0.22-0.18 (s, 48H) (See Scheme 1A and Figure S2 and S3).

Synthesis of POSS2. *Tert*-butyl acetoacetate (TBAA, 5.78 mL, 34.9 mmol, 8.80 equiv) was added to a 50 mL RBF containing OBA-POSS (8.23 g, 3.96 mmol, 1.00 equiv) and a stir bar. The RBF was equipped with a distillation apparatus and stirred at room temperature for 10 min. After, the RBF was submerged in a 120 °C oil bath and stirred for 12 h. The reaction mixture was then placed under reduced pressure to vacuum distill off the excess TBAA at 130 °C for 4 h, yielding a very viscous yellow oil with slight excess dark, extremely viscous brown oil with slight excess TBAA present. The product was used without further purification (10.2 g, 93.2%). ¹H NMR (CDCl₃, 600 MHz): δ 4.18–4.10 (t, 14 H), 3.45–3.40 (s, 14H), 2.28–2.25 (s, 21 H), 1.70–1.60 (p, 16H), 0.65–0.58 (t, 16H), 0.22–0.18 (s, 48H) (Scheme 1B and Figure S6–7).

General Preparation of POSS1 Vitrimers. POSS1 (87.5% functionalized, 1.00 g, 0.483 mmol, 1.00 equiv) was loaded into a Petri dish and dissolved in THF (8 mL). In a separate vial, diamine (1.86 mmol, 3.85 equiv) was diluted with 2 mL of THF. The diamine solution was added to the Petri dish, and the solvent was evaporated at room temperature overnight. For vitrimer cross-linked with DADD, the diamine was heated with a heat gun until mostly solubilized. The DADD solution was rapidly added to the Petri dish. An additional 2 mL of THF was added to the DADD vial, heated, and added to the Petri dish. The resulting films were further cured at 85 °C for 6 h under vacuum. The cured vitrimer films were ground, and

Crosslinker POSS1 POSS2

m-Xylyenediamine (XDA)

Hexamethylenediamine (HMDA)

Diaminododecane (DADD)

D1

Chart 1. Vitrimer Formulations and Naming Conventions of POSS1 and POSS2 Crosslinked with Various Diamines

compression molded at 160 °C under reduced pressure, yielding yellow, transparent materials (Figure 2 and Figures S8 and S27).

General Preparation of POSS2 Vitrimers. POSS2 (87.5% functionalized, 1.00 g, 0.362 mmol, 1.00 equiv) was loaded into a Petri dish and dissolved in THF (8 mL). In a separate vial, diamine (1.39 mmol, 3.85 equiv) was diluted with 2 mL of THF. The diamine solution was added to the Petri dish, and the solvent was evaporated at room temperature overnight. For vitrimer cross-linked with DADD, the diamine was heated with a heat gun until mostly solubilized. The DADD solution was rapidly added to the Petri dish. An additional 2 mL of THF was added to the DADD vial, heated, and added to the Petri dish. The resulting films were cured at 85 °C for 6 h under vacuum. The cured vitrimer films were ground, and compression molded at 160 °C under reduced pressure, yielding brownish yellow, transparent materials. (Figure 3; Figures S11 and S31).

Characterization. NMR spectroscopy was used to characterize monomers and their monomer precursors. FTIR spectroscopy, and X-ray diffraction (XRD) were used to characterize the polymers. Thermogravimetric analysis (TGA), differential scanning calorimetry (DSC), atmospheric thermal degradation, and chemical degradation were conducted to evaluate thermochemical properties. Dynamic mechanical analysis (DMA), creep-recovery, and stress-relaxation were conducted to observe mechanical and viscoelastic behavior. Swelling experiments evaluated solvent resistance and mesh size/swelling ratios. The Archimedes method was utilized for density measurements. The experimental details are summarized in the Supporting Information.

RESULTS AND DISCUSSION

Synthesis and Characterization of POSS Derivatives and Nanocomposite Vitrimers. We sought to fabricate enaminone-cross-linked vitrimers while maintaining a high level of POSS filler content, anticipating this would result in vitrimers that could be easily shaped and reprocessed yet provide robust thermomechanical stability, features demonstrated by Liang and co-workers in their report on a dynamic covalent elastomer composite with excellent ablative properties. 64 We further hypothesized that with high POSS loadings these networks would provide significant char yields following pyrolysis. Therefore, POSS derivatives possessing multiple β ketoester functional groups were synthesized to allow covalent incorporation of the inorganic cage into vitrimers using simple commercial diamines. The degree of functionality of the POSS precursor should lead to a dense step-growth network capable of high resistance to deformation (creep) at elevated temperatures, a necessity for potential HSM candidates. We envisioned that an aliphatic (propyl) or aromatic (benzyl) spacer could be integrated into β -ketoester POSS derivatives to allow for variability in thermomechanical properties of the vitrimer and overall char yield of the pyrolyzed material. To this end, nanocage monomers were prepared via a facile and high-yielding two-step synthesis from commercially available OctaSilane-POSS (H-POSS). While H-POSS is not strictly speaking a POSS cage, rather a Q₈M₈^H octadimethyl cubic

silane, the ease of monomer synthesis is favorable over the hydrolytic condensation of trialkoxy-/chlorosilanes necessary to form true POSS cages. To prepare the two β -ketoester POSS cages, H-POSS was first subjected to platinum-catalyzed hydrosilylation with a slight excess (10 mol %) of either allyl alcohol (POSS1) or 4-vinylbenzyl alcohol (POSS2) (Scheme 1 and Figures S1 and S4). The resultant neat viscous oils were then treated with tert-butylacetoacetate (TBAA) to furnish cages bearing, on average, seven β -ketoester groups as determined by ¹H NMR analysis (Figures S2 and S5). Finally, FTIR spectroscopy indicated the absence of an -OH stretching band and the presence of a C=O stretching band from the β -ketoester functional groups (Figures S6 and S7). We suspect that with higher excess of TBAA in the alcoholysis step, full functionalization of the POSS cage is likely achievable. However, we found even at this extent of excess, the high viscosity of the POSS1/2 monomers make it extremely difficult to remove the residual TBAA even under reduced pressure and elevated temperatures.

The nanocomposite vitrimers were then prepared via stepgrowth polycondensation, cross-linking POSS1 or POSS2 with various diamines. Specifically, to investigate the consequences of diamine spacer length and flexibility on material properties, we prepared vitrimers X1 or 2 from *m*-xylylene diamine (XDA), H1 or 2 from hexamethylene diamine (HMDA), and D1 or 2 from diaminododecane (DADD), where the number 1 or 2 refers to materials prepared from POSS1 or POSS2, respectively (Chart 1).

Since HSMs require robust dimensional stability at high operational temperatures, the POSS derivatives were cross-linked with only 10 mol % excess of amino groups, providing network materials with appreciable shapeability and reprocess-ability yet sufficient resistance to creep at elevated temperature. Vitrimers were synthesized in a straightforward solution-cast protocol from tetrahydrofuran and cured at 85 °C under reduced pressure. After curing, the vitrimers were broken into shards and compression molded into discs and bars at 160 °C under vacuum to give transparent and homogeneous materials (Figure 2A–G and Figures S27–S33).

X-ray diffraction (XRD) of the processed vitrimer discs showed a consistently amorphous broad peak in the range of $2\Theta \approx 14.5-27^\circ$ (Figure 3A and Figures S21–S26). The lack of distinct crystalline signals indicates that the nanofillers are homogeneously distributed with minimal POSS–POSS cage interactions that could lead to aggregation or heterogeneity at the macroscopic level; however, the existence of aggregates at the micron level is possible and would require analysis via electron microscopy. The vitrimer films were then characterized by thermogravimetric analysis (TGA), differential scanning calorimetry (DSC), FTIR spectroscopy, dynamic mechanical analysis (DMA), and shear rheology.

FTIR spectroscopy of all the vitrimers showed complete disappearance of the C=O stretching bands of the β -ketoester at ~1725 cm⁻¹ and displayed the characteristic signals for the formation of enaminones at ~ 1600 and ~ 1650 cm⁻¹, corresponding to the C=C stretching and N-H bending, respectively. Additionally, retention of the signal at ~1075 cm⁻¹ was observed in all cases, corresponding to POSS Si-O-Si stretching (Figure 3B and Figures S8-S13). DSC analysis indicated that the $T_{\rm g}$ of the nanocomposites was indeed influenced by the functionality of the cage vertices and the nature of the diamine cross-linker (Figure 3C, D and Figures S14–S19). The T_g values of POSS1 vitrimers ranged from 23 to 39 °C, while those of POSS2 vitrimers were higher, ranging from 39 to 73 °C. The relatively similar length of the XDA and HMDA cross-linkers led to comparable $T_{\rm g}$ values for vitrimers prepared from POSS1 (39 and 37 °C, respectively) and POSS2 (73 and 66 °C, respectively). Since vitrimers made with HMDA displayed only slightly lower values of T_g than their XDA counterparts, we conclude that the observed differences in T_{σ} values between POSS1 and POSS2 vitrimers are due to the higher degrees of freedom of the aliphatic spacer in the POSS1 precursors, resulting in an increase in segmental mobility of the polymer matrix. As expected, both D1 and D2, having been cross-linked with the longest and most flexible diamine, displayed dramatically lower $T_{\rm g}$ values (23 and 39 °C, respectively). Notably, vitrimer D1 remained flexible at room temperature after compression molding (Figure S30). Selected properties of all vitrimer samples are shown in Table 1.

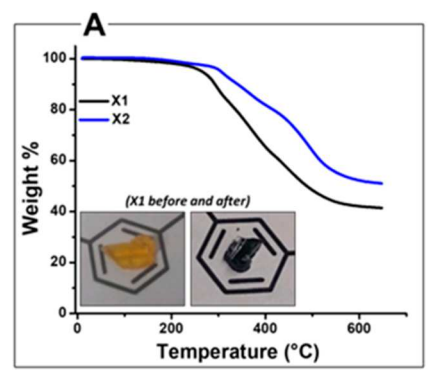
Table 1. Selected Preliminary Properties of POSS Vitrimers

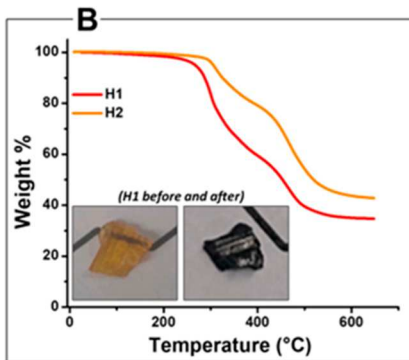
Sample	Storage modulus at 160 °C (MPa)	T_{gDSC} ($^{\circ}\mathrm{C}$)	$T_{g,\mathrm{DMA}}$ (°C)	$T_{ m d,5\%~mass~loss}$	Char yield at 650 °C(N_2) (%)	Inorganic/ POSS content (wt %)
X1	32	39	57	265	41	54
H1	49	37	55	267	35	55
D1	34	23	40	256	28	41
X2	18	73	76	305	51	40
H2	27	66	75	305	43	43
D2	16	39	56	312	38	34

Thermooxidative Stability and Shape Retention. Thorough TGA studies were conducted to test the thermal

stability of the POSS-containing vitrimers. The vitrimers were initially heated to a maximum temperature of 650 °C under an inert atmosphere to gain insight into the degradation profiles of the various formulations prior to complete ablation of carbon content. The POSS1 vitrimers displayed modest degradation temperatures (i.e., temperature at which 5% mass loss is reached, $T_{
m d, 5\%}$) of 265, 267, and 256 °C and demonstrated char yields of 41, 35, and 28% for X1, H1, and D1, respectively (Figure 4A-C). Multiple modes of degradation were evidenced for the POSS1 aliphatic derivatives. Gratifyingly, the final char material for POSS1 vitrimers appeared to retain the distinct shape of the sample prior to decomposition. D1 seemed to show the best retention of detail despite its overall decrease in volume and mass loss. As expected, the increased aromatic character of the POSS2 formulations affected both the $T_{
m d, 5\%}$ and char yield, with onset temperatures of 305, 305, and 312 °C and char yields of 51, 43, and 38% for X2, H2, and D2, respectively (Figure 4A-C).

We next extended the thermal stability studies beyond 1000 °C, conditions more relevant to potential HSM applications. For all of the vitrimers, heating to 1150 °C in a dual TGA/ DSC experiment (under N₂) displayed no appreciable change in the final char yield as compared to the preliminary thermal stability tests (Figure \$35-\$40), and the materials again showed similar retention of the original shape (Figure S60). The POSS1 materials possessed two distinct decomposition modes (Figure S41). The first decomposition mode was similar between X1 and H1, with D1 being the most pronounced in both rate and magnitude of decomposition, a consequence of higher aliphatic carbon content and resulting lower network density. Such molecular features clearly govern the final char yield of the materials under inert atmosphere. Furthermore, all POSS1 vitrimers showed DSC thermograms with three distinct exotherms (Figures S42-44). The first and smallest occurs at approximately 300 °C, where the major decomposition of bare H-POSS begins (Figure S34) ($T_{\rm d, 5\%}$ = 309 °C), as well as the approximate start of the onset temperatures of the POSS1 vitrimers. This is likely attributable to thermal cracking of the POSS core and subsequent crosslinking of Si-O residues.⁶⁷ The second and larger exotherms all occur roughly at 450 °C (nearly the same as the onset of the second decomposition), a result of carbonization of the organic component of the network. The most pronounced exotherm





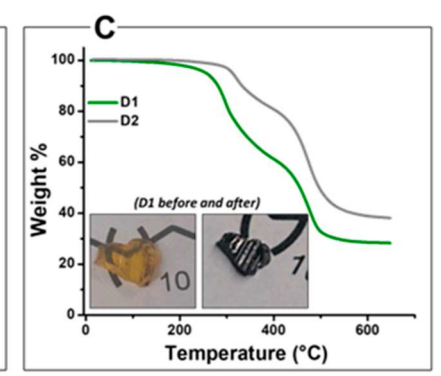


Figure 4. Low-temperature (N_2) thermogravimetric analysis (TGA) plots of (A) POSS1 (β-ketoester functionalized cage with an aliphatic spacer) and POSS2 (β-ketoester functionalized cage with an aromatic spacer) cages cross-linked with m-xylyenediamine (X1 and 2, respectively); (B) hexamethylenediamine (H1 and H2, respectively) and (C) diaminododecane (D1 and D2, respectively). TGA plots indicate that onset of degradation temperature ($T_{\rm d, 5\%}$) and char yield (plateau regions at 650 °C) are tunable by nature of POSS vertices (aliphatic versus aromatic) and diamine cross-linker.

occurred at approximately 600–700 °C, likely a crystallization event leading to a carbonaceous amorphous glass. The high-temperature TGA results for POSS2 vitrimers mostly agree with the lower temperature results (Figures S44–S46); however, X2 displays a slow but constant degradation profile, lacking any distinct exotherms in comparison to all other formulations (Figures S45–S47). In fact, the char yield at 1150 °C is lower than its POSS1 counterpart. The comparatively higher aromatic content in X2 leads to an extended carbonization event. H2 and D2 again showed increased $T_{\rm d}$ and char yields compared to H1 and D1, with comparable exotherms occurring slightly higher at 700–800 °C.

The atmospheric stability of the vitrimers was tested at temperatures up to 1100 °C. Each sample was placed on an alumina plate in air and heated to the designated temperature at 10 °C/min. The samples were held at the designated temperature for 12 h before natural cooling to room temperature (the furnace was turned off but left closed). Relying on the previously obtained TGA/DSC data, each sample was heated at 300, 650, and 1100 °C (Figure S49). After heating to 300 °C, all samples became black and shrunk in size, with some curling at the edges (Figure S55). POSS1 vitrimers appeared to retain the pattern from the Teflon tape used during compression molding, again with D1 appearing to have the best retention as seen in preliminary TGA studies. Moreover, no notable change in size was observed after the 650 or 1100 °C exposures. All formulas were brittle after the 650 °C exposure; however, the small, tough crystals remained difficult to crush for FT-IR analysis after treatment at 650 and 1100 °C.

Regardless of which POSS monomer or diamine was used for the nanocomposite vitrimer, the nanofiller cage seemingly allows for stabilization of the organic content over long heating periods as well as predictable char yields. Yet, TGA results in Figure S38 suggest that X2 is a slight outlier in that there are diminishing returns on aromatic content; the char material lacked any plateau in weight percent or distinct exotherm near 600–700 °C in the DSC thermogram. We hypothesize that the increased aromatic character results in significantly higher carbon content remaining present at these temperatures, disrupting the crystallization events occurring in the other vitrimer samples that leads to the final inert char as evidenced by clear plateaus.

FT-IR analysis of D1 over the course of the heating process showed clear evidence for the formation of an amorphous glass (Figure 5). After 12 h at 300 °C, the material showed distinct C-H stretching signals overlapping with the virgin materials as well as a subtle, broad absorption at approximately the frequency of the enaminone functional groups. After 12 h at 650 °C, the material was nearly completely white and consequently all organic signals were lost in the IR spectrum. Interestingly, after the treatment at 1100 °C, the Si-O stretching showed a minor shift to a higher wavenumber, potentially indicating a new phase of the amorphous silica. Silica is a complex polymorph that demonstrates a variety of glassy and crystalline phases with some overlap of temperature ranges. However, given the long dwell time at 300, 650, and 1100 °C, we expect that tridymite, quartz, and cristobalite, respectively, are the most likely phases to be present, though more in-depth DSC and XRD analysis is required.

Vitrimer Density and Mesh Size Determination. Nanocomposite vitrimer density was measured (×3) by Archimedes' principle using eq S1 (Figure 6A and Table

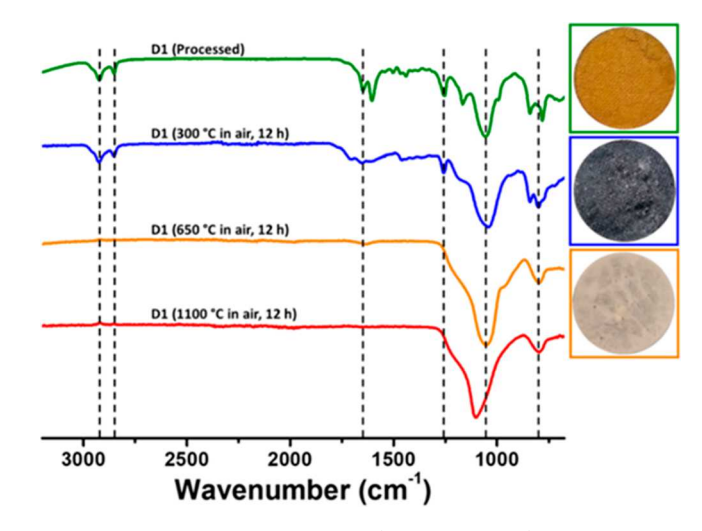
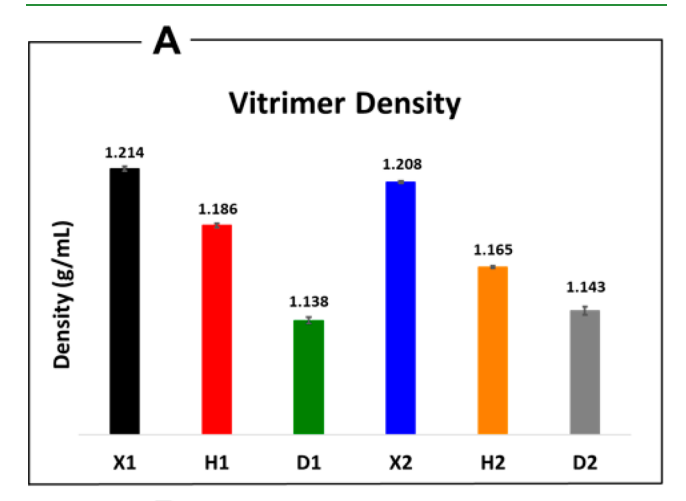


Figure 5. FTIR spectra of POSS1 (aliphatic spacer) vitrimer cross-linked with diaminododecane (D1) before and after heating to 300, 650, and $1100\,^{\circ}\text{C}$ (top to bottom, respectively).



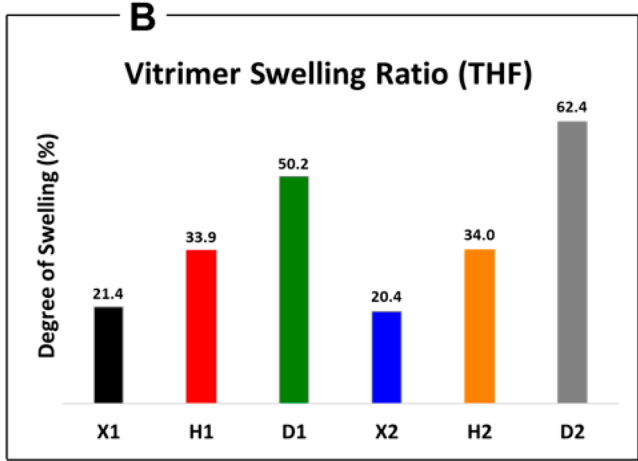


Figure 6. (A) Density of vitrimers as determined by Archimedes' test and (B) swelling ratios as determined by immersion in THF for 48 h.

S3). A clear relationship was observed between the vitrimer densities and the length and flexibility of the diamine cross-linker, where densities range from 1.214 to 1.138 g/mL for POSS1 samples and 1.208 to 1.143 g/mL for POSS2 samples.

To validate the measured density values for the vitrimers, the samples were then swollen in THF for 48 h, with the solvent

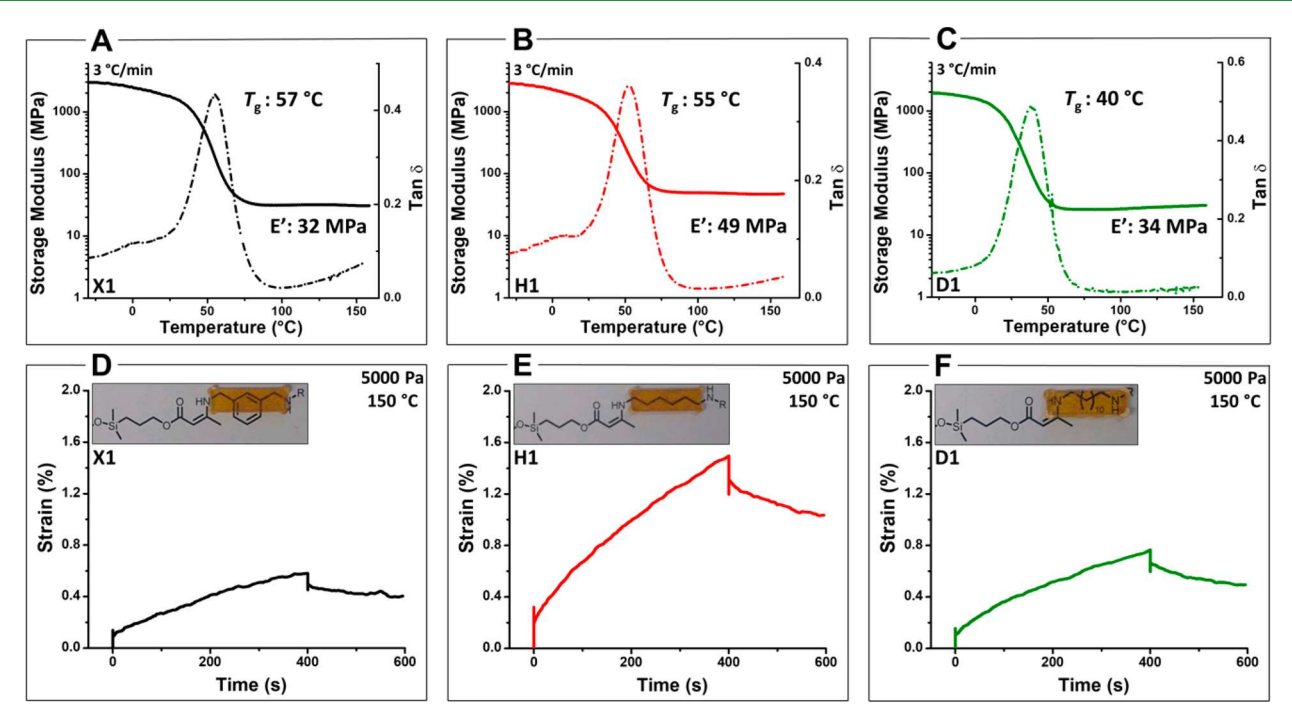


Figure 7. Creep-recovery experiments for (A) X1, (B) H1, and (C) D1 vitrimers at 150 $^{\circ}$ C at a constant force of 5000 Pa (vitrimer samples ran in duplicate) showing excellent creep resistance and DMA thermograms of (D) X1, (E) H1, and (F) D1 vitrimers showing T_g values and constant rubbery plateau moduli.

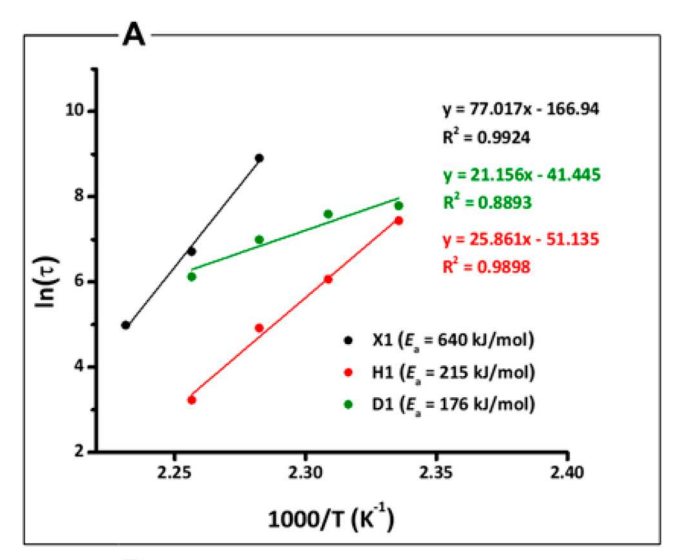
removed and replenished after 24 h (other solvents tested such as ethanol, methanol, and diethyl ether gave no appreciable swelling after 48 h). The swelling percentages were notably small for all vitrimers, offering further evidence of their highly densified network structure (Figure 6B). Gratifyingly, the trends in swelling percentages were consistent with the measured densities and indicated a predictable inorganic network density that scaled inversely with the length/flexibility of the diamine cross-linker. In addition to their shapability, the density of these materials (comparable to PMMA) and their solvoresistance potentially make them attractive materials for lightweight, weather-resistant thermal protective barriers.

Rheological Properties. The thermomechanical properties of the nanocomposite vitrimers were evaluated by DMA. Cross-linked networks were evidenced by the rubbery plateaus observed in all DMA thermograms, displaying constant crosslink density over a 100 °C range past $T_{\rm g}$ for all POSS1 and POSS2 samples (Figure 7A-C and Figures S66-S74, respectively). Markedly, the rubbery plateau moduli were exceptionally high for all POSS1 vitrimers, indicating that the network structures were notably dense, a consequence of the high connectivity and rigidity of the POSS cage repeat unit. Typically, an increase in cross-link density-observed by an increase in the storage modulus (E') of the rubbery plateau corresponds with a rise in T_g as the segmental mobility of the polymer is restricted. The \check{T}_{α} of the vitrimers determined by DMA and DSC exhibited a strong dependence on the length and flexibility of the diamine cross-linker, decreasing slightly from the XDA vitrimers to HMDA vitrimers and more dramatically for the vitrimers cross-linked with the lengthy dodecyl spacer of DADD. Interestingly, the E' of X1 did not trend as expected, resulting in the lowest E' of the three POSS1 vitrimers even though X1 contained the shortest and most rigid cross-linker. We hypothesize that the higher degrees of freedom/flexibility of the aliphatic diamines could lead to

loop catenations of cross-links, artificially increasing the observed cross-link density.

Resistance to deformation at elevated temperatures was evaluated by conducting creep-recovery experiments at 150 °C under 5 kPa of force. The vitrimers all displayed excellent resistance to the applied deformation. After 400 s, the POSS1 vitrimers reached maximum strains ranging from 0.58 to 1.5% and had similar recoveries of approximately 30% (Figure 7D–F). The POSS2 materials also displayed similar resistance to creep, reaching maximum strains between 1.3 and 1.6% (Figures S75–S77). However, the elasticity of H2 and D2 was markedly pronounced, showing a dramatic increase in deformation followed by an instantaneous rebound of the material before entering the viscous flow regime. Moreover, the apparent recovery was significantly higher than the POSS1 counterparts and appeared to scale similarly to the extent of the initial elastic deformation.

Stress relaxation experiments were conducted to probe the temperature sensitivity (or energy of activation for viscous flow, E_a) of the vitrimer networks. Given the creep data, we were unsurprised to observe extremely long characteristic relaxation times (τ , time when $G/G_0 = 1/e$) (Figure S78–85). We applied stress-relaxation data to Arrhenius' law, assuming a single Maxwell model, by plotting $ln(\tau)$ versus inverse temperature and extracting E_a from the slope (eq S2). POSS1 vitrimers had disparate E_a values ranging from 176 to 640 kJ/mol (Figure 8A). These data indicate that the temperature sensitivity of the nanocomposite vitrimers (comparable to magnitude of E_a and the slope of the linear regression fit) corresponds to the nature of the diamine (length and rigidity/flexibility). Furthermore, the much higher E_a values for these vitrimer composites compared to previously reported enaminone vitrimers confirm a dramatic decrease in flow behavior as a result of the dense network composition and structural rigidity of the POSS nanocage. It is worth noting



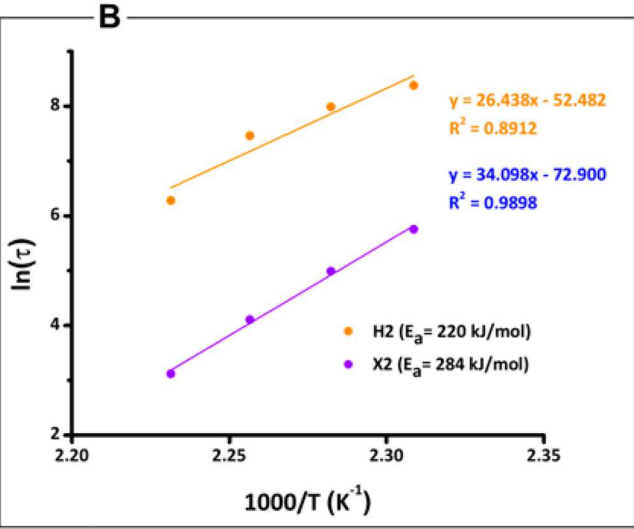


Figure 8. Arrhenius plots of stress relaxation data for (A) POSS1 and (B) POSS2 vitrimers (τ at $G/G_0 = 1/e$, in 5 °C increments). Data indicate sluggish flow behavior, largely dependent on diamine functionality. Vitrimer samples were ran in duplicate.

that X1 could only be plotted with three temperature points due to inability to reach its characteristic relaxation time below 165 °C and yielded an unusually high $E_{\rm a}$ value in comparison to analogous CAN systems. While temperatures exceeding 175 °C could be probed, we observed rapid discoloration of the materials at such elevated temperatures, which we attribute to decomposition or oxidation of the amine content (Figure S86). Furthermore, the relaxation curves for D1 do not obey typical logarithmic decay and the data points deviate from linearity, indicating complex flow behavior that does not obey an Arrhenius relationship (Figures S81 and S82). Similarly sluggish stress relaxation was demonstrated by the X2 and H2 vitrimers (Figure 8B), while D2 failed to reach its characteristic relaxation time below 175 °C (Figure S83).

The particularly high weight percent of inorganic filler, the high degree of functionality of the POSS cages, and the relatively low mol % excess amine led to dramatically perturbed vitrimer flow behavior. These results suggest there may be limitations to filler weight percent in dynamic nanocomposites, with flow potentially being dictated more by the nanofiller than the dynamic component. Nevertheless,

flow could potentially be enhanced by increasing the excess amine content, which has also be shown to illicit an effect on the mechanism of cross-link exchange.³⁹ Typically, this would be seen as a considerable drawback for a vitrimer system. However, considering the harsh (deformative force and/or elevated temperatures) and long-term storage conditions HSMs are subjected to, these vitrimers may be suitable for use as additive components to thermal protection systems.

Reprocessability and Mild Chemical Degradation. To evaluate the reprocessability of the networks, we conducted DMA studies to measure the E' and $T_{\rm g}$ of bars of the virgin networks that were broken and healed up to four times for the POSS1 vitrimers. The first two reprocess cycles (Rx1 and Rx2) were conducted at 160 °C with the subsequent two at 175 °C, due to the increase in $T_{\rm g}$ after two cycles. Values of the plateau storage modulus were extrapolated from the rubbery plateau region of the thermogram, and values of $T_{\rm g}$ were measured at the peak of $\tan(\delta)$ (Figures S87–S104). X1 showed a slight increase in both $T_{\rm g}$ and rubbery plateau modulus over reprocessing cycles, likely a result of amine oxidation and subsequent loss of the productive species for exchange. H1 showed the least consistent reprocessability with variability in $T_{\rm g}$ and E' across healing cycles. Gratifyingly, D1 showed good reprocessability, with only a moderate increase in the $T_{\rm g}$ and good retention of the original E' over each healing cycle.

The reprocessability of the POSS2 vitrimers was less notable than that of POSS1, as efficient healing could only be achieved up to three cycles for only the X1 vitrimer. Nevertheless, the reprocessed bars appeared to have only relatively minor defects accumulating after healing and retained good transparency (Figure S104). FTIR analysis of reprocessed bars of both POSS1 and POSS2 vitrimers were near identical with the virgin material, indicating retention of the enaminone functional group and inorganic cage (Figure S105–110). We suspect the lability of the benzylic carbon of the ester could be contributing to the marked decrease in reprocessability of the POSS2 vitrimers, which could be a site for permanent crosslink formation via $S_{\rm N}2$ displacement by free amines.

Another attractive feature of dynamic covalent networks is the potential for chemical degradation and recycling. The enaminone bond has been shown to degrade efficiently in the presence of excess monofunctional amine. 43,44 Additionally, the bond is hydrolytically labile under acidic conditions. Therefore, we chose X1 to observe mild degradation by both methods (Figure S111). No swelling or dissolution was observed when a disk of X1 was submerged in THF for 48 h. The addition of either hexylamine or aqueous HCl resulted in the vitrimers being near completely solubilized with trace amounts of intractable solids (Figure S112). These results suggest the POSS nanocomposite vitrimers can also be effectively degraded under mild conditions, allowing for facile end-of-life management and potential chemical recycling.

CONCLUSIONS

ı

Nanocomposite vitrimers are an emerging platform for fabricating dynamic covalent networks with enhanced material properties, thermooxidative stability, and reprocessability. Until recently, POSS-based vitrimers have found only limited use as scaffolds for designing such nanocomposites. These results demonstrate new routes for the synthesis and utility of multifunctional β -ketoester-POSS nanocages for the fabrication of novel nanocomposite enaminone vitrimers of diverse architectures. The final vitrimer properties can be tuned by

virtue of the POSS-vertex functionality (aliphatic versus aromatic) and the choice of multiamine cross-linker. Indeed, the structure-property relationships elucidated in these studies indicate that such nanocomposite vitrimer materials can be specifically designed for rapid reprocessability to give largely defect-free films with excellent transparency, thermal stability, char yield, adjustable T_g , and facile shapeability. Following thermal degradation up to 650 °C in N₂ and 300 °C in air, the final char materials showed marked retention of the imprinted shape of the parent material. Moreover, their complex network structure endowed the networks with a strong resistance to deformation at elevated temperature. One caveat, however, is that the remarkably high weight percent of POSS filler may retard relaxation of shear stress, indicating a threshold above which flow behavior is particularly hampered. The thermomechanical behavior of these POSS vitrimers is under continued investigation, but given our initial findings, we believe these nanocomposite vitrimers could serve as a useful platform for designing heat-shielding materials capable of straightforward shapeability.

ASSOCIATED CONTENT

Supporting Information

The Supporting Information is available free of charge at https://pubs.acs.org/doi/10.1021/acsami.2c22924.

> Materials and instrumentation, POSS synthesis and characterization, vitrimer synthesis, rheology, reprocessing, chemical recycling, and references (PDF)

AUTHOR INFORMATION

Corresponding Author

Brent S. Sumerlin – George & Josephine Butler Polymer Research Laboratory, Center for Macromolecular Science & Engineering, Department of Chemistry, University of Florida, Gainesville, Florida 32611, United States; o orcid.org/ 0000-0001-5749-5444; Email: sumerlin@chem.ufl.edu

Authors

Kevin A. Stewart - George & Josephine Butler Polymer Research Laboratory, Center for Macromolecular Science & Engineering, Department of Chemistry, University of Florida, Gainesville, Florida 32611, United States

Daniel P. DeLellis - Department of Materials Science and Engineering, University of Florida, Gainesville, Florida 32603, United States; orcid.org/0000-0002-6080-7004

Jacob J. Lessard – George & Josephine Butler Polymer Research Laboratory, Center for Macromolecular Science & Engineering, Department of Chemistry, University of Florida, Gainesville, Florida 32611, United States; o orcid.org/ 0000-0003-2962-6472

John F. Rynk – Department of Materials Science and Engineering, University of Florida, Gainesville, Florida 32603, United States

Complete contact information is available at: https://pubs.acs.org/10.1021/acsami.2c22924

Author Contributions

The manuscript was written through contributions of all authors. All authors have given approval to the final version of the manuscript.

Notes

The authors declare no competing financial interest.

ACKNOWLEDGMENTS

This material is based upon work supported by the National Science Foundation (NSF DMR-1904631). We thank Anton Paar for the use of the Anton Paar 702 rheometer through their VIP academic program.

REFERENCES

- (1) Long, T. E. Toward Recyclable Thermosets. Science 2014, 344,
- (2) George, K.; Panda, B. P.; Mohanty, S.; Nayak, S. K. Recent Developments in Elastomeric Heat Shielding Materials for Solid Rocket Motor Casing Application for Future Perspective. Polym. Adv. Technol. 2018, 29, 8-21.
- (3) Natali, M.; Kenny, J. M.; Torre, L. Science and Technology of Polymeric Ablative Materials for Thermal Protection Systems and Propulsion Devices: A Review. Prog. Mater. Sci. 2016, 84, 192-275.
- (4) Donskoy, A. Elastomeric Heat-Shielding Materials for Internal Surfaces of Missile Engines. Int. J. Poly. Mater. 1996, 31, 215-236.
- (5) Natali, M.; Monti, M.; Puglia, D.; Kenny, J. M.; Torre, L. Composites: Part A Ablative Properties of Carbon Black and MWNT/Phenolic Composites: A Comparative Study. Compos. Part A 2012, 43, 174-182.
- (6) Nayak, N. V. Composite Materials in Aerospace Applications. Int.I. Sci. Res. Publ. 2014, 4, 1-10.
- (7) Qu, H.; Hui, K.; Bian, C.; Guan, Y.; Li, H.; Luan, T.; Yan, N. Lightweight and Mechanically Robust EPDM Foams for High Thermal Insulation and Moderate Ablative Resistance Via Constructing Cellular Char Layer. Macrol. Mater. Eng. 2022, 307, 2100665.
- (8) Moore, L. M. J.; Greeson, K. T.; Stewart, K. A.; Kure, D. A.; Corley, C. A.; Jennings, A. R.; Iacono, S. T.; Ghiassi, K. B. Perfluoropyridine as a Scaffold for Semifluorinated Thiol-Ene Networks with Readily Tunable Thermal Properties. Macromol. Chem. Phys. 2020, 221, 2000100.
- (9) Li, J.; Hu, B.; Hui, K.; Li, K.; Wang, L. Effects of Inorganic Nanofibers and High Char Yield Fillers on Char Layer Structure and Ablation Resistance of Ethylene Propylene Diene Monomer Composites. Compos. Part A 2021, 150, 106633.
- (10) Kabra, S.; Tandon, S.; Kandasubramanian, B. POSS Nanocomposites for Defense and Space Applications. Polyhedral Oligomeric Silsesquioxane (POSS) Polymer Nanocomposites. 2021, 481–498.
- (11) Eismeier, S.; Peloquin, A. J.; Stewart, K. A.; Corley, C. A.; Iacono, S. T. Pyridine-Functionalized Linear and Network Step-Growth Fluoropolymers, I. Fluor, Chem. 2020, 238, 109631.
- (12) Jia, X.; Zeng, Z.; Li, G.; Hui, D.; Yang, X.; Wang, S. Enhancement of Ablative and Interfacial Bonding Properties of EPDM Composites by Incorporating Epoxy Phenolic Resin. Compos. Part B 2013, 54, 234-240.
- (13) Singh, S.; Guchhait, P. K.; Bandyopadhyay, G. G.; Chaki, T. K. Development of Polyimide - Nanosilica filled EPDM Based Light Rocket Motor Insulator Compound: Influence of Polyimide -Nanosilica Loading on Thermal, Ablation, and Mechanical Properties. Compos. Part A 2013, 44, 8-15.
- (14) Yang, D.; Zhang, W.; Jiang, B.; Guo, Y. Silicone Rubber Ablative Composites Improved with Zirconium Carbide or Zirconia. Compos. Part A 2013, 44, 70-77.
- (15) Guan, Y.; Zhang, L. X.; Zhang, L. Q.; Lu, Y. L. Study on Ablative Properties and Mechanisms of Hydrogenated Nitrile Butadiene Rubber (HNBR) Composites Containing Different Fillers. Polym. Degrad. Stab. 2011, 96, 808-817.
- (16) George, K.; Mohanty, S.; Biswal, M.; Nayak, S. K. Thermal Insulation Behaviour of Ethylene Propylene Diene Monomer Rubber/ Kevlar Fiber Based Hybrid Composites Containing Nanosilica for Solid Rocket Motor Insulation. J. Appl. Polym. Sci. 2021, 138, 49934. (17) Winne, J. M.; Leibler, L.; Du Prez, F. E. Dynamic Covalent Chemistry in Polymer Networks: A Mechanistic Perspective. Polym.

Chem. 2019, 10, 6091-6108.

- (18) Montarnal, D.; Capelot, M.; Tournilhac, F.; Leibler, L. Silicalike Malleable Materials from Permanent Organic Networks. *Science* **2011**, 334, 965–968.
- (19) Guerre, M.; Taplan, C.; Winne, J. M.; Du Prez, F. E. Vitrimers: Directing Chemical Reactivity to Control Material Properties. *Chem. Sci.* **2020**, *11*, 4855–4870.
- (20) Scheutz, G. M.; Lessard, J. J.; Sims, M. B.; Sumerlin, B. S. Adaptable Crosslinks in Polymeric Materials: Resolving the Intersection of Thermoplastics and Thermosets. *J. Am. Chem. Soc.* **2019**, *141*, 16181–16196.
- (21) Chen, X.; Dam, M. A.; Ono, K.; Mal, A.; Shen, H.; Nutt, S. R.; Sheran, K.; Wudl, F. A Thermally Re-Mendable Cross-Linked Polymeric Material. *Science* **2002**, *295*, 1698–1702.
- (22) Gheneim, R.; Perez-berumen, C.; Gandini, A. Diels Alder Reactions with Novel Polymeric Dienes and Dienophiles: Synthesis of Reversibly Cross-Linked Elastomers. *Macromolecules* **2002**, *35*, 7246–7253.
- (23) Taplan, C.; Guerre, M.; Du Prez, F. E. Du. Covalent Adaptable Networks Using β Amino Esters as Thermally Reversible Building Blocks. *J. Am. Chem. Soc.* **2021**, *143*, 9140–9150.
- (24) Elling, B. R.; Dichtel, W. R. Reprocessable Cross-Linked Polymer Networks: Are Associative Exchange Mechanisms Desirable? *ACS Cent. Sci.* **2020**, *6*, 1488–1496.
- (25) Mondal, S.; Lessard, J. J.; Meena, C. L.; Sanjayan, G. J.; Sumerlin, B. S. Janus Cross-Links in Supramolecular Networks. *J. Am. Chem. Soc.* **2022**, *144*, 845–853.
- (26) Zhang, L.; Rowan, S. J. Effect of Sterics and Degree of Cross-Linking on the Mechanical Properties of Dynamic Poly(Alkylurea-urethane) Networks. ACS Macro Lett. 2017, 50, 5051–5060.
- (27) Van Zee, N. J.; Nicolaÿ, R. Vitrimers: Permanently Crosslinked Polymers with Dynamic Network Topology. *Prog. Polym. Sci.* **2020**, 104, 101233.
- (28) Spiesschaert, Y.; Taplan, C.; Stricker, L.; Guerre, M.; Winne, J. M.; Du Prez, F. E. Influence of the Polymer Matrix on the Viscoelastic Behaviour of Vitrimers. *Polym. Chem.* **2020**, *11*, 5377–5385.
- (29) Wu, S.; Chen, Q. Advances and New Opportunities in the Rheology of Physically and Chemically Reversible Polymers. *Macromolecules* **2022**, *55*, 697–714.
- (30) Maassen, E. E. L.; Heuts, J. P. A.; Sijbesma, R. P. Reversible Crosslinking and Fast Stress Relaxation in Dynamic Polymer Networks via Transalkylation Using 1,4-Diazabicyclo [2.2.2] Octane. *Polym. Chem.* **2021**, *12*, 3640–3649.
- (31) Wang, Y.; Pan, Y.; Zheng, Z.; Ding, X. Reconfigurable and Reprocessable Thermoset Shape Memory Polymer with Synergetic Triple Dynamic Covalent Bonds. *Macromol. Rapid Commun.* **2018**, 39, 1800128.
- (32) Self, J. L.; Dolinski, N. D.; Zayas, M. S.; Read De Alaniz, J.; Bates, C. M. Brønsted-Acid-Catalyzed Exchange in Polyester Dynamic Covalent Networks. *ACS Macro Lett.* **2018**, *7*, 817–821.
- (33) Self, J. L.; Sample, C. S.; Levi, A. E.; Li, K.; Xie, R.; De Alaniz, J. R.; Bates, C. M. Dynamic Bottlebrush Polymer Networks: Self-Healing in Super-Soft Materials. *J. Am. Chem. Soc.* **2020**, *142*, 7567–7573.
- (34) Nishimura, Y.; Chung, J.; Muradyan, H.; Guan, Z. Silyl Ether as a Robust and Thermally Stable Dynamic Covalent Motif for Malleable Polymer Design. *J. Am. Chem. Soc.* **2017**, *139*, 14881–14884.
- (35) Van Lijsebetten, F.; Holloway, J. O.; Winne, J. M.; Du Prez, F. E. Internal Catalysis for Dynamic Covalent Chemistry Applications and Polymer Science. *Chem. Soc. Rev.* **2020**, *49*, 8425–8438.
- (36) Cash, J. J.; Kubo, T.; Bapat, A. P.; Sumerlin, B. S. Room-Temperature Self-Healing Polymers Based on Dynamic-Covalent Boronic Esters. *Macromolecules* **2015**, 48, 2098–2106.
- (37) Wang, S.; Ma, S.; Li, Q.; Yuan, W.; Wang, B.; Zhu, J. Robust, Fire-Safe, Monomer-Recovery, Highly Malleable Thermosets from Renewable Bioresources. *Macromolecules* **2018**, *51*, 8001–8012.
- (38) Geng, H.; Wang, Y.; Yu, Q.; Gu, S.; Zhou, Y.; Xu, W.; Zhang, X.; Ye, D. Vanillin-Based Polyschiff Vitrimers: Reprocessability and Chemical Recyclability. ACS Sustain. Chem. Eng. 2018, 6, 15463—15470.

- (39) Denissen, W.; Rivero, G.; Nicolaÿ, R.; Leibler, L.; Winne, J. M.; Du Prez, F. E. Vinylogous Urethane Vitrimers. *Adv. Funct. Mater.* **2015**, 25, 2451–2457.
- (40) Guerre, M.; Taplan, C.; Nicolaÿ, R.; Winne, J. M.; Du Prez, F. E. Fluorinated Vitrimer Elastomers with a Dual Temperature Response. *J. Am. Chem. Soc.* **2018**, *140*, 13272–13284.
- (41) Spiesschaert, Y.; Guerre, M.; De Baere, I.; Van Paepegem, W.; Winne, J. M.; Du Prez, F. E. Dynamic Curing Agents for Amine-Hardened Epoxy Vitrimers with Short (Re)Processing Times. *Macromolecules* **2020**, *53*, 2485–2495.
- (42) Wang, S.; Li, L.; Liu, Q.; Urban, M. W. Self-Healable Acrylic-Based Covalently Adaptable Networks. *Macromolecules* **2022**, *55*, 4703–4709.
- (43) Lessard, J. J.; Garcia, L. F.; Easterling, C. P.; Sims, M. B.; Bentz, K. C.; Arencibia, S.; Savin, D. A.; Sumerlin, B. S. Catalyst-Free Vitrimers from Vinyl Polymers. *Macromolecules* **2019**, *52*, 2105–2111.
- (44) Lessard, J. J.; Scheutz, G. M.; Hughes, R. W.; Sumerlin, B. S. Polystyrene-Based Vitrimers: Inexpensive and Recyclable Thermosets. *ACS Appl. Polym. Mater.* **2020**, *2*, 3044–3048.
- (45) Lessard, J. J.; Scheutz, G. M.; Sung, S. H.; Lantz, K. A.; Epps, T. H.; Sumerlin, B. S. Block Copolymer Vitrimers. *J. Am. Chem. Soc.* **2020**, *142*, 283–289.
- (46) Lessard, J. J.; Stewart, K. A.; Sumerlin, B. S. Controlling Dynamics of Associative Networks through Primary Chain Length. *Macromolecules* **2022**, *55*, 10052–10061.
- (47) Yang, Y.; Xu, Y.; Ji, Y.; Wei, Y. Functional Epoxy Vitrimers and Composites. *Prog. Mater. Sci.* **2021**, *120*, 100710.
- (48) Kamble, M.; Vashisth, A.; Yang, H.; Pranompont, S.; Picu, C. R.; Wang, D.; Koratkar, N. Reversing Fatigue in Carbon- Fi Ber Reinforced Vitrimer Composites. *Carbon* **2022**, *187*, 108–114.
- (49) Ghosh, B.; Urban, W. M. Self-Repairing Oxetane-Substituted Chitosan Polyurethane Networks. *Science* **2009**, 323, 1458–1460.
- (50) Fang, H.; Ye, W.; Yang, K.; Song, K.; Wei, H.; Ding, Y. Vitrimer Chemistry Enables Epoxy Nanocomposites with Mechanical Robustness and Integrated Conductive Segregated Structure for High Performance Electromagnetic Interference Shielding. *Compos. Part B* **2021**, 215, 108782.
- (51) Swartz, J. L.; Li, R. L.; Dichtel, W. R. Incorporating Functionalized Cellulose to Increase the Toughness of Covalent Adaptable Networks. ACS Appl. Mater. Interfaces 2020, 12, 44110–44116.
- (52) Liu, Y.; Wang, B.; Ma, S.; Yu, T.; Xu, X.; Li, Q.; Wang, S.; Han, Y.; Yu, Z.; Zhu, J. Catalyst-Free Malleable, Degradable, Bio-Based Epoxy Thermosets and Its Application in Recyclable Carbon Fiber Composites. *Compos. Part B Eng.* **2021**, *211*, 108654.
- (53) Wang, S.; Ma, S.; Li, Q.; Xu, X.; Wang, B.; Yuan, W.; Zhou, S.; You, S.; Zhu, J. Facile: In Situ Preparation of High-Performance Epoxy Vitrimer from Renewable Resources and Its Application in Nondestructive Recyclable Carbon Fiber Composite. *Green Chem.* **2019**, *21*, 1484–1497.
- (54) Luo, S.; Ma, Y.; Wei, X.; Jin, Y.; Qiu, L.; Zhang, W. Malleable and Recyclable Vitrimer Graphene Aerogel Composite with High Electrical Conductivity. ACS Appl. Electron. Mater. 2021, 3, 1178–1183.
- (55) Chen, X.; Li, L.; Wei, T.; Venerus, D. C.; Torkelson, J. M. Reprocessable Polyhydroxyurethane Network Composites: Effect of Filler Surface Functionality on Cross-Link Density Recovery and Stress Relaxation. ACS Appl. Mater. Interfaces 2019, 11, 2398–2407.
- (56) McMullin, E.; Rebar, H. T.; Mather, P. T. Biodegradable Thermoplastic Elastomers Incorporating POSS: Synthesis, Microstructure, and Mechanical Properties. *Macromolecules* **2016**, *49*, 3769–3779.
- (57) Stewart, K. A.; Shuster, D.; Leising, M.; Coolidge, I.; Lee, E.; Stevens, C.; Peloquin, A. J.; Kure, D.; Jennings, A. R.; Iacono, S. T. Synthesis, Characterization, and Thermal Properties of Fluoropyridyl-Functionalized Siloxanes of Diverse Polymeric Architectures. *Macromolecules* **2021**, *54*, 4871–4879.

- (58) Liu, H.; Zheng, S. Polyurethane Networks Nanoreinforced by Polyhedral Oligomeric Silsesquioxane. *Macromol. Rapid Commun.* **2005**, *26*, 196–200.
- (59) Mettry, M.; Worthington, M. A.; Au, B.; Forien, J. B.; Chandrasekaran, S.; Heth, N. A.; Schwartz, J. J.; Liang, S.; Smith, W.; Biener, J.; Saha, S. K.; Oakdale, J. S. Refractive Index Matched Polymeric and Preceramic Resins for Height-Scalable Two-Photon Lithography. *RSC Adv.* **2021**, *11*, 22633–22639.
- (60) Devaraju, S.; Vengatesan, M. R.; Selvi, M.; Kumar, A. A.; Alagar, M. Synthesis and Characterization of Bisphenol-A Ether Diamine-Based Polyimide POSS Nanocomposites for Low K Dielectric and Flame-Retardant Applications. *High Perform. Polym.* **2012**, *24*, 85–96.
- (61) Yang, H.; He, C.; Russell, T. P.; Wang, D. Epoxy-Polyhedral Oligomeric Silsesquioxanes (POSS) Nanocomposite Vitrimers with High Strength, Toughness, and Efficient Relaxation. *Giant* **2020**, *4*, 100035.
- (62) Hajiali, F.; Tajbakhsh, S.; Marić, M. Thermally Reprocessable Bio-Based Polymethacrylate Vitrimers and Nanocomposites. *Polymer* **2021**, *212*, 123126.
- (63) Zhao, B.; Hang, G.; Li, L.; Zheng, S. Nanocomposites of Polyethylene with Polyhedral Oligomeric Silsesquioxane: From Thermoplastics to Vitrimers through Silyl Ether Metathesis. *Mater. Today Chem.* **2022**, 24, 100759.
- (64) Hu, S.; Chen, X.; Bin Rusayyis, M. A.; Purwanto, N. S.; Torkelson, J. M. Reprocessable Polyhydroxyurethane Networks Reinforced with Reactive Polyhedral Oligomeric Silsesquioxanes (POSS) and Exhibiting Excellent Elevated Temperature Creep Resistance. *Polymer* 2022, 252, 124971.
- (65) Cai, Y.; Zou, H.; Zhou, S.; Chen, Y.; Liang, M. Room-Temperature Self-Healing Ablative Composites via Dynamic Covalent Bonds for High-Performance Applications. *ACS Appl. Polym. Mater.* **2020**, *2*, 3977–3987.
- (66) Liu, W.; Hang, G.; Mei, H.; Li, L.; Zheng, S. Nanocomposites of Polyhydroxyurethane with POSS Microdomains: Synthesis via Non-Isocyanate Approach, Morphologies and Reprocessing Properties. *Polymers* **2022**, *14*, 1331.
- (67) Fina, A.; Tabuani, D.; Carniato, F.; Frache, A.; Boccaleri, E.; Camino, G. Polyhedral Oligomeric Silsesquioxanes (POSS) Thermal Degradation. *Thermochim. Acta* **2006**, *440*, 36–42.
- (68) Schnurre, S.M.; Grobner, J.; Schmid-Fetzer, R. Thermodynamics and Phase Stability in the Si O System. *J. Non. Cryst. Solids* **2004**, 336, 1–25.
- (69) Haida, P.; Abetz, V. Acid-Mediated Autocatalysis in Vinylogous Urethane Vitrimers. *Macromol. Rapid Commun.* **2020**, *41*, 2000273.